

A Coupled Electrical Resistivity–Infiltration Model for Wetting Front Evaluation

Dale Rucker*

A coupled resistivity–infiltration model was developed. The infiltration model relies on the analytical solution of a fully developed and sharp wetting front using the Green–Ampt approximation, thereby reducing the resistivity model to the simple two-layer case. The Green–Ampt approximation is a highly simplistic soil model that has limited applicability to real soils. The forward model demonstrates the effects of a voltage drop with time for a pole–pole, Wenner, and dipole–dipole electrode arrangement for a moving wetting front. The velocity of the wetting front can be obtained directly from the time series curve by normalizing the measured apparent resistivity to the resistivity of the wet layer (estimated from the voltage at time $t = \infty$) and plotting against the reciprocal of time multiplied by the electrode separation. Furthermore, if the cumulative infiltration or other parameters are known, then the hydraulic conductivity can be calculated.

THE USE OF geophysical data to evaluate hydrologic events has been an area of growing research during the past decade (e.g., Eppstein and Dougherty, 1998; Alumbaugh et al., 2002; Singha and Gorelick, 2006). In this new study area of hydrogeophysics, the geophysical method is usually applied as a characterization tool to map the subtle spatial variability in the physical properties of the earth. Through a correlation of known conditions to measured responses (e.g., Archie, 1942; Feng and Sen, 1985), the geophysical data are remapped as hydrogeologic variables of water content (Topp et al., 1980), hydraulic conductivity (Slater and Glaser, 2003), porosity (Bosch, 2004), or clay content and salinity (de Lima and Niwas, 2000; Shevvin et al., 2007).

A repeated set of geophysical measurements with time may yield information regarding the transient nature of water movement in the subsurface. Geophysics as a monitoring tool is particularly useful for defining those hydrologic variables that are rate dependent, such as hydraulic conductivity or velocity of a

moving wetting front during infiltration. By including the temporal information from the geophysical measurements and directly coupling with a transient hydrologic analysis, the estimation of hydraulic conductivity can be improved over transformative analysis with geophysical data at a single snapshot in time.

Several studies have used time-lapse geophysical monitoring for defining hydrologic variables. Binley et al. (2002) used time-lapse geophysical measurements of both electrical resistivity and ground penetrating radar (GPR) to calibrate a numerical model of water movement in the vadose zone. French and Binley (2004) measured the changes in resistivity with time to calculate the changes in saturation during snowmelt. Lambot et al. (2004) used a surface-based GPR and full wave form electromagnetic wave modeling to estimate the hydraulic parameters of the van Genuchten soil-water characteristic curve. Singha and Gorelick (2005) compared spatial moments from NaCl transport modeling to electrical resistivity tomography measurements. Kowalsky et al. (2005) used multiple geophysical data sets in a joint inversion to create a better representation of the water content distribution with time. Cassiani et al. (2006) used time-lapse resistivity to infer the hydrologic mechanisms of double porosity and high permeability zones during a saline tracer test. Oldenborger et al. (2007) tracked a tracer plume into an unconfined aquifer through an injection and withdrawal experiment to predict a recoverable solute mass. These studies relied on several discrete snapshots of the geophysical data, where the time between snapshots, Δt_m , was probably determined by convenience (equipment availability, time of station reoccupation, length of measurement cycle, etc.). Recently, Furman et al. (2007) demonstrated an approach that

hydroGEOPHYSICS, Inc., 2302 N. Forbes Blvd., Tucson, AZ 85745. Received 1 Apr. 2008. *Corresponding author (drucker@hgiworld.com).

Vadose Zone J. 8:383–388
doi:10.2136/vzj2008.0080

© Soil Science Society of America
677 S. Segoe Rd. Madison, WI 53711 USA.
All rights reserved. No part of this periodical may be reproduced or transmitted in any form or by any means, electronic or mechanical, including photocopying, recording, or any information storage and retrieval system, without permission in writing from the publisher.

could reduce Δt_m by focusing the measurements in the most sensitive areas using an optimization technique. Their optimization technique reduced the total number of measurements, thereby reducing the length of the measurement cycle.

In this work, we developed a coupled direct current electrical resistivity–infiltration solution to define hydraulic variables in the limit as $\Delta t_m \rightarrow 0$, thereby morphing the time-lapse monitoring scenario into a continuous monitoring scenario. In this analysis, the one-dimensional infiltration solution relied on a set of simplifying assumptions of (i) a sharp and flat wetting front described as the Green–Ampt approximation (Green and Ampt, 1911) and (ii) a fully developed wetting front so that its velocity was constant throughout infiltration. The sharp wetting front created a two-layer resistivity geometry, where the depth to the bottom layer changed with time, depending on the hydraulic conductivity of the soil and the boundary conditions. Two closely related studies (Rucker and Ferré, 2004; Ferré et al., 2006) presented a similar method of time series analysis to obtain hydraulic parameters. This study differed significantly from past work by presenting a solution that allows direct computation of the hydraulic parameters, as opposed to non-linear optimization that searches for the best set of parameters.

Theory

One-Dimensional Infiltration

Consider the one-dimensional vertical infiltration of water from the surface presented in Fig. 1a. The soil is initially unsaturated and is characterized by an initial pressure head (h_{dry}), water content (θ_{dry}), and hydraulic conductivity ($K_{dry} \sim 0$). Wetting occurs instantaneously and water at the soil surface is ponded to a depth h_0 . The ponded height also represents the pressure head at the soil surface. The water percolates downward and the lower edge of the wetting front is located z_f below the ground surface. Ahead of the wetting front, the initial soil conditions remain unchanged. Behind the wetting front, the water content increases to a constant value of θ_{wet} , with a corresponding h_{wet} and K_{wet} .

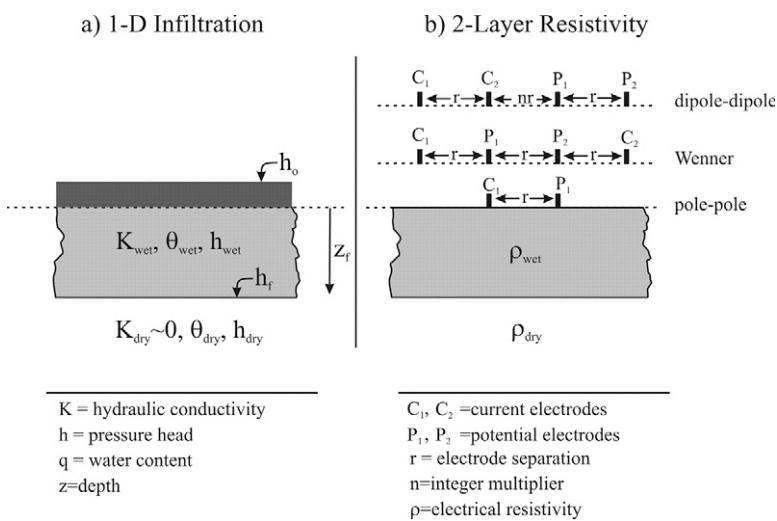


FIG. 1. Geometry and parameters of (a) the vertical infiltration model, and (b) the two-layer resistivity model; h_{dry} , θ_{dry} , K_{dry} , and ρ_{dry} are the dry-region pressure head, water content, hydraulic conductivity, and resistivity, respectively; h_{wet} , θ_{wet} , K_{wet} , and ρ_{wet} are the pressure head, water content, hydraulic conductivity, and resistivity, respectively, behind the wetting front.

to form a rectangular pulse. The sharp changes in the hydraulic parameters at the wetting front were considered by Green and Ampt (1911) as a first-order approximation to the infiltration problem and is most applicable to coarse-grained soils.

The infiltration flux rate, i , for the Green–Ampt scenario is

$$i = K_{wet} \left(1 + \frac{\Delta h}{z_f} \right) \quad [1]$$

where Δh is the change in pressure head, $h_0 - h_p$ and h_f is the pressure head at the wetting front. Using conservation of mass, the cumulative infiltration, C (per unit area of infiltration) is

$$C = i dt = \Delta \theta z_f \quad [2]$$

where $\Delta \theta$ is the difference in water content, $\theta_{wet} - \theta_{dry}$, and t is time. For small t , the position of the wetting front can be approximated by (Warrick, 2003)

$$\frac{K_{wet} t}{\Delta \theta} \sim z_f - \Delta h \left[\frac{z_f}{\Delta h} - \frac{1}{2} \left(\frac{z_f}{\Delta h} \right)^2 \right] \quad [3]$$

For large time, the fully developed wetting front will approach a constant velocity of

$$\frac{dz_f}{dt} = \frac{K_{wet}}{\Delta \theta} \quad [4]$$

and the transition from early to late time is marked by the characteristic time, t_g :

$$t_g = \left(\frac{S}{K_{wet}} \right)^2 \quad [5]$$

$$S = \left[2K_{wet} (\theta_{wet} - \theta_{dry}) (h_{wet} - h_f) \right]^{0.5} \quad [6]$$

The parameter S is called the sorptivity (a function of boundary and soil conditions) and $h_{wet} - h_f$ is equal to the capillary length. The capillary length can be thought of as an air-entry pressure into a fully water-saturated soil. In coarse soils, the capillary length is short, allowing the wetting front to fully develop relatively early. The extension of this study to more complex solutions of infiltration is trivial given that Eq. [4] has been demonstrated to hold true by several researchers, including Philip (1969) and Warrick (1993).

The use of the Green–Ampt soil model has been shown to be of limited value for real and complex field applications. The sharp transition of the wetting front is actually more diffuse for more commonly used soil-water characteristic curves such as the Brooks–Corey or van Genuchten forms. Additionally, the characteristic time to transition from a variable to a constant wetting front velocity between the different forms to describe a soil will cause the Green–Ampt to generally underestimate the position relative to other forms. Its usage here is to demonstrate a very simplified analysis to allow direct coupling of the resistivity and infiltration equations, and subsequently the inverse calculation for hydraulic conductivity.

One-Dimensional Electrical Potential for a Two-Layer Model

Continuing with the hydraulic example of a sharp wetting front moving downward at a constant velocity of $K_{\text{wet}}/\Delta\theta$, an arbitrary electrical resistivity array is placed over the infiltration region and a continuous time series data set of voltage potentials is recorded. For familiarity, we demonstrate the pole–pole, Wenner, and dipole–dipole responses; however, the voltage potential about any arrangement of the general four-electrode array can be calculated from the basic pole–pole data.

Using Fig. 1b as a reference, the solution for the voltages measured over a two-layered earth from the pole–pole array (V_{pp}) on the earth surface with an electrode separation of r is (Wait, 1982):

$$V_{\text{pp}}(r) = \frac{I\rho_{\text{wet}}}{2\pi r} G(r, z_f, R) \quad [7]$$

where I is the electrical current, G is the two-layer kernel, and R is the reflection coefficient comprised of a function of the wet-region electrical resistivity (ρ_{wet}) and dry-region resistivity (ρ_{dry}):

$$R = \frac{\rho_{\text{dry}} - \rho_{\text{wet}}}{\rho_{\text{dry}} + \rho_{\text{wet}}} \quad [8]$$

For the case of an infiltration, $\rho_{\text{wet}} < \rho_{\text{dry}}$ and R will necessarily vary between 0 and 1. The two-layer kernel, G , is

$$G(r, z_f, R) = 1 + 2Rr \int_0^\infty \frac{\exp(-2z_f\lambda)}{1 - R\epsilon(-2z_f\lambda)} J_0(\lambda r) d\lambda \quad [9]$$

where J_0 is the Bessel function of the first kind of order zero and λ is a dummy variable of integration. Equation [9] can be simplified to an infinite series per Kunetz (1966) and Wait (1982):

$$G(r, z_f, R) = 1 + 2Rr \sum_{j=0}^{\infty} \frac{R^j}{\left\{ r^2 + [(2j+2)z_f]^2 \right\}^{0.5}} \quad [10]$$

Expansion of the measured voltage at the surface from Eq. [7] to the Wenner (V_{Wen}) and dipole–dipole (V_{dd}) arrays is completed through superposition:

$$V_{\text{Wen}}(r) = \frac{I\rho_{\text{wet}}}{2\pi} \left[\frac{2G(r, z_f, R)}{r} - \frac{G(2r, z_f, R)}{2r} \right] \quad [11]$$

$$V_{\text{dd}}(r) = \frac{I\rho_{\text{wet}}}{2\pi} \left\{ \left[\frac{G(nr, z_f, R)}{nr} - \frac{G(r+nr, z_f, R)}{r+nr} \right] - \left[\frac{G(nr, z_f, R)}{nr} - \frac{G(2r+nr, z_f, R)}{2r+nr} \right] \right\} \quad [12]$$

Equation [12] was established with the n factor of increasing dipole separation as shown in Fig. 1b to keep the equation generic. For this work, however, I've set $n = 1$ for simplicity.

Since the position of the wetting front is a function of time, we can couple the infiltration equation with Eq. [7] and [10] to obtain

$$V_{\text{pp}}(r, t) = \frac{I\rho_{\text{wet}}}{2\pi r} \left(1 + 2Rr \sum_{j=0}^{\infty} \frac{R^j}{\left\{ r^2 + [(2j+2)(K_{\text{wet}}/\Delta\theta)t]^2 \right\}^{0.5}} \right) \quad [13]$$

It is clear from Eq. [13] that when $t = 0$, $G(r, z_f, R) \rightarrow 1 + [2R/(1 - R)] = \rho_{\text{dry}}/\rho_{\text{wet}}$ and the voltage is that from a dry, homogeneous earth. Conversely, as t approaches infinity, $G(r, z_f, R) \rightarrow 1$ and the voltage is derived from a wet earth.

Example

Forward Model of Voltage Potential during Infiltration

The voltage potential during infiltration with time was calculated for a soil with the following hydraulic properties: $K_{\text{wet}} = 0.34$ m/h, $K_{\text{dry}} \sim 0$ m/h, $\theta_{\text{wet}} = 0.287$ m³/m³, and $\theta_{\text{dry}} = 0.1$ m³/m³, with a velocity of the wetting front of 1.8182 m/h. As a simplification for the resistivity model, the $\rho_{\text{wet}} = 10$ Ω-m, and $\rho_{\text{dry}} = 100$ Ω-m. These specific resistivity values can be obtained from an exponential relationship to water content by

$$\rho_{\text{soil}} = \rho_{\text{water}} \theta^{-m} \quad [14]$$

where $m = 2.184$ and $\rho_{\text{water}} = 0.655$ Ω-m. Schon (1996) referred to this petrophysical relation as the “second Archie Equation,” where the parameter m is the saturation exponent. Conceivably, other petrophysical models can be used to convert water content to electrical resistivity (e.g., Waxman and Smits, 1968), which account for more realistic surface conduction along grain-to-grain contacts. The use of Archie's equation above was for simplicity and to reduce the total number of parameters.

A hypothetical pole–pole, Wenner, and dipole–dipole monitoring survey was conducted over the infiltration area. The monitoring survey consisted simply of the four electrodes fixed at the earth's surface. The distance between the near-field electrodes were equal among the array types (Fig. 1b), which was set to the distance of travel of the wetting front after 1 h. The injection current was also held constant at 1 amp.

Figure 2a shows the modeled results for the three arrays from 0 to 80 h. The figure shows a monotonically decreasing function for all arrays. The dipole–dipole array was more sensitive to the moving wetting front (as compared by the temporal derivative of the voltage) at early times, but had a lower signal strength than the pole–pole or Wenner arrays. The minimum voltage occurred when the wetting front reached a depth equal to 1 h of infiltration, after which the dipole–dipole array could not see the characteristics of the wetting front any longer. The Wenner also appears to have had little sensitivity after the wetting front had passed 1 h of infiltration. The pole–pole array had a generally lower sensitivity at early times but higher sensitivity at late times. The array was capable of tracking the wetting front at relatively late time.

Figure 2b demonstrates the measured voltage for different geometric and soil properties for the pole–pole array. The original pole–pole data set from Fig. 2a is reproduced in Fig. 2b and comparisons are made for a faster soil ($2K_{\text{wet}}$) and a larger electrode separation ($3r$). The larger separation is equivalent to the positions of the outer electrodes for the Wenner and dipole–dipole arrays. As expected, the signal strength of the large electrode separation was much lower than those of the smaller separations. The simulation with the fast and slow hydraulic conductivity began and ended with the same voltage values.

For direct comparisons among the data sets, the time series data were converted to dimensionless forms by normalizing the

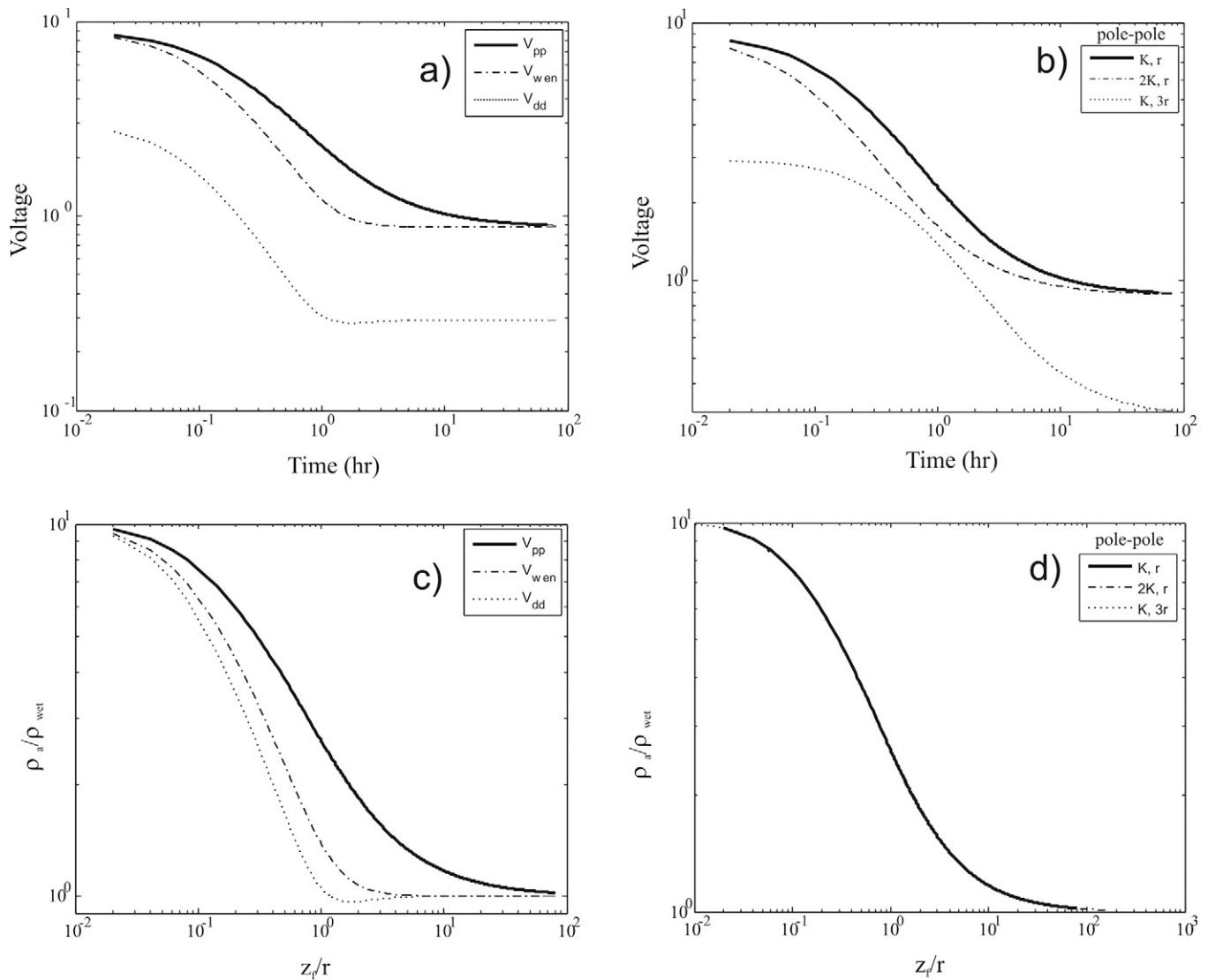


FIG. 2. Voltage measurements (a) while monitoring a moving wetting front using the pole–pole (V_{pp}), Wenner (V_{wen}), and dipole–dipole arrays (V_{dd}), and (b) for different hydraulic conductivity (K) and electrode separations (r) using the pole–pole array; plots of dimensionless parameters of (c) the data in (a), and (d) the data in (b).

measured voltage. The normalization was conducted by converting the voltage to the apparent resistivity and dividing by the resistivity of the wet region. The time axis is replaced by z_f/r , the relative distance of travel of the wetting front to the electrode spacing. Figure 2c and 2d show the normalized plots from Fig. 2a and 2b, respectively. The sensitivity of the normalized dipole–dipole and Wenner arrays in Fig. 2c are very similar, with the Wenner seeing slightly beyond one electrode spacing. The pole–pole array was capable of imaging far beyond the depth equivalent of one electrode spacing, with 3.55% of the maximum signal left after the wetting front had passed a depth of five electrode spacings. The pole–pole array is known for its ability to see deeper into the subsurface with lower sensitivity to targets (Roy and Apparo, 1971).

The normalized resistivity ρ_a/ρ_{wet} is equal to the two-layer kernel, G . Figure 2d specifically shows that $G(1, z_f/r, R)$ is equivalent for all of the pole–pole examples that changed wetting velocity (through an increase in K_{wet}) or electrode separations. In a special case, where the depth of the wetting front is equal to the electrode spacing, G reduces to

$$G(R) = 1 + 2 \sum_{j=0}^{\infty} \frac{R^j}{[1 + 4(j+1)^2]^{0.5}} \quad [15]$$

and Fig. 3 shows the function $G(R)$ for the pole–pole, dipole–dipole, and Wenner arrays.

Inverse Model to Determine Hydraulic Properties Directly from Measured Electrical Data

In the case presented above, the time series data sets can be mined for specific quantities to help solve the inverse problem for extraction of hydraulic parameters. First, the end states of completely dry or wet are essentially homogeneous resistivity problems and the apparent resistivity will be equal to the true resistivity. Calculation of the ρ_{wet} and ρ_{dry} will lead to the calculation of the reflection coefficient, R . Once R is established, $G(R)$ can be computed. To simplify the computation of G , a rational polynomial was fit to each curve in Fig. 3 to establish the following:

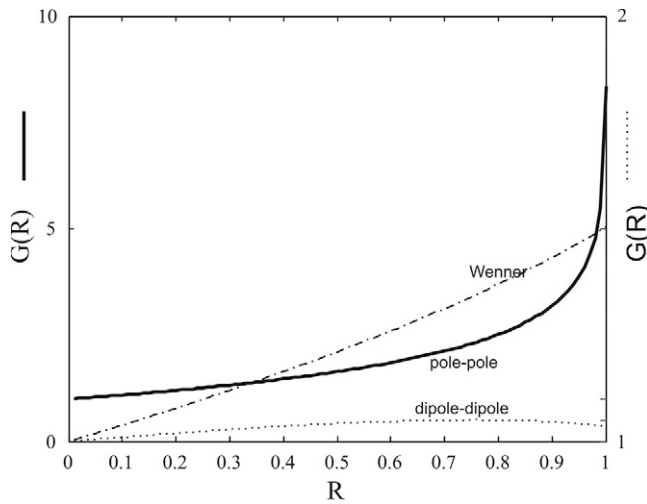


FIG. 3. The dimensionless two-layer kernel $G(R)$ as a function of the reflection coefficient R for the pole–pole, Wenner, and dipole–dipole arrays.

$$G_{pp}(R) = \frac{p_1 R + p_2}{R^3 + q_1 R^2 + q_2 R + q_3} \quad [16]$$

$$p_1 = -20.32, p_2 = 20.57$$

$$q_1 = 12.59, q_2 = -33.46, q_3 = 19.9$$

$$G_{Wen}(R) = c_1 R^3 + c_2 R^2 + c_3 R + c_4 \quad [17]$$

$$c_1 = 0.1112, c_2 = -0.00476$$

$$c_3 = 0.3968, c_4 = 0.9987$$

$$G_{dd}(R) = d_1 R^3 + d_2 R^2 + d_3 R + d_4 \quad [18]$$

$$d_1 = -0.09303, d_2 = 0.04463$$

$$d_3 = 0.08453, d_4 = 1.001$$

Figure 4a shows the fit for the pole–pole model. Given the ρ_{wet} and ρ_{dry} from the time series curve, $R = 0.8181$ and $G(R) = 2.604$. The normalized time-series electrical data of Fig. 4b demonstrate that $G(R)$ does in fact land at $z_f/r = 1$. It is impossible to make use of this curve further, however, due to the simple fact that we do not know anything about z_f . Substitution of Eq. [4] for z_f and rearranging to establish an abscissa that is more useful,

$$\frac{K_{wet}}{\Delta\theta} = \frac{r}{t} \Big|_{G(R)} \quad [19]$$

yields Fig. 4c. Equation [19] shows that when r/t is evaluated at $G(R)$, the velocity of the wetting front can be calculated. In this case, the velocity is 1.8182 m/h, equal to the known velocity.

The method of estimating the wetting front velocity for the pole–pole array can easily be extended to the other array types mentioned here. Since both Wenner and dipole–dipole arrays are sensitive to a depth of at least one electrode spacing, the transformation shown in Eq. [19] can be readily applied to all voltage data within Fig. 2a. In some circumstances, it may be desirable to use the Wenner array over the pole–pole and dipole–dipole arrays given (i) the high signal strength of the measurement over the dipole–dipole method, and (ii) the shortened time to reach $t = \infty$ for estimating ρ_{wet} relative to the pole–pole array. Given the large footprint needed by the Wenner array relative to the pole

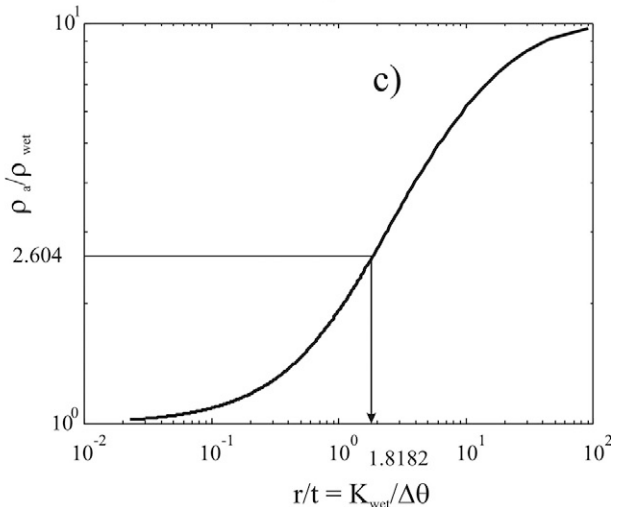
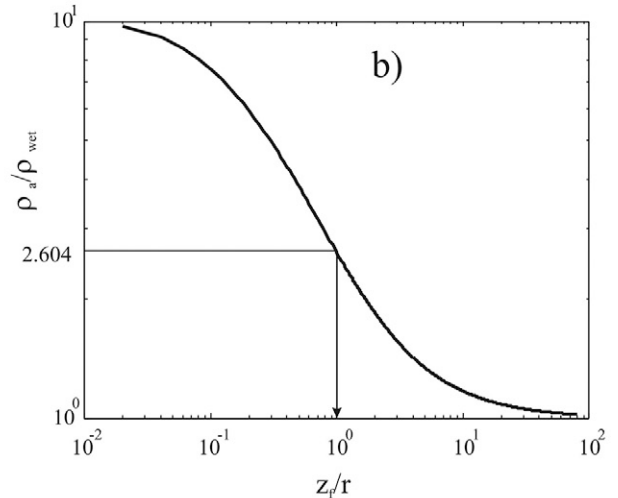
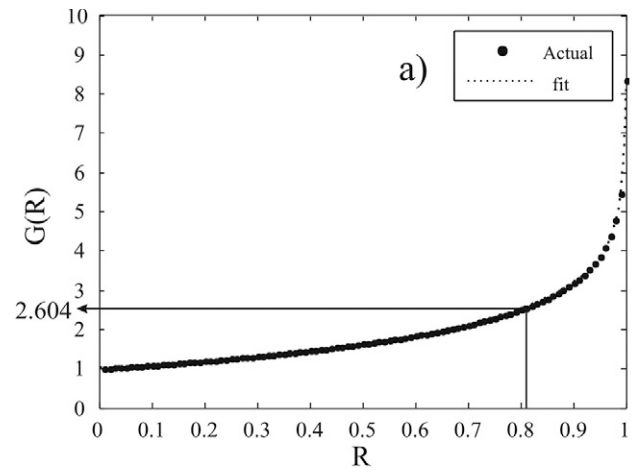


FIG. 4. (a) Demonstration of the rational polynomial fit to the dimensionless two-layer kernel $G(R)$ for the pole–pole array; (b) verification of the validity of the dimensionless two-layer kernel; and (c) a graphical method to determine the wetting front velocity from the normalized apparent resistivity (ρ_a/ρ_{wet}), evaluated at the dimensionless two-layer kernel. z_f/r , the relative distance of travel of the wetting front to the electrode spacing ($r/t = K_{wet}/\Delta\theta$).

pole array, however, a larger infiltration area would be required to ensure one-dimensional infiltration.

Further analysis to obtain the hydraulic conductivity will take much more work. A priori knowledge of the specific

parameters that comprise Eq. [14] would yield both θ_{wet} and θ_{dry} , and the hydraulic conductivity could be computed using their difference. It is not an unreasonable request to ask that the researchers of infiltration obtain the electrical conductivity of the infiltrating water, $1/\rho_{\text{water}}$, thereby reducing the number of unknown parameters in Eq. [14] to one. Furthermore, given the fair-allotment issues arising from the scarcity of water resources in many semiarid regions, the cumulative infiltration volume is probably a parameter that is recorded carefully. In this case, Eq. [2] can be used to obtain the $\Delta\theta$, allowing direct computation of the hydraulic conductivity from Eq. [19]. Lastly, parameter estimation techniques that explore parameter space using nonlinear least squares inversion could be used to search for the unique parameter set of K_{wet} , ρ_{water} , and m . Additional constraints such as a precalculated wetting front velocity could narrow down the prospective field of possible solution sets very quickly.

Conclusions

A coupled electrical resistivity–infiltration model was developed from the analytical solutions describing the Green–Ampt approximation of a sharp wetting front and the two-layer resistivity model. The coupled model demonstrated the effects on time series data from continuously monitoring the voltage drop while the wetting front moved downward through the earth. The demonstration was facilitated by using the pole–pole, Wenner, and dipole–dipole electrode arrangements.

The direct comparisons among the array types were accomplished by normalizing the voltage and time axes. The comparisons showed that once the wetting front passed the equivalent depth of one electrode spacing, the dipole–dipole array became insensitive to further movement. For the Wenner array, the voltage measurement became insensitive after the wetting front progressed to two electrode spacings. The pole–pole array was sensitive to a wetting front at least 10 electrode spacings deep.

The normalized ordinate axis of the time series plot reduced to the two-layer resistivity kernel. A special dimensionless case of the two-layer kernel was evaluated by setting the depth of the wetting front and the electrode separation to a value of one. The dimensionless two-layer kernel can be evaluated simply by knowing the homogeneous resistivity end states at $t = 0$ and $t = \infty$. From the dimensionless kernel, the velocity of the wetting front, $K_{\text{wet}}/\Delta\theta$, can be graphically determined, demonstrating that hydrogeologic parameters can be obtained directly from geophysical measurements. Since the measurements of each of the array types tested is sensitive to a depth of at least one electrode spacing, any array type would be suitable for monitoring. Furthermore, if the cumulative infiltration is known (a parameter likely to be tracked by researchers), or the parameters that describe the constitutive relationship between resistivity and water content can be measured, then hydraulic conductivity can be calculated.

References

Alumbaugh, D., P.Y. Chang, L. Paprocki, J.R. Brainard, R.J. Glass, and C.A. Rautman. 2002. Estimating moisture contents in the vadose zone using cross-borehole ground penetrating radar: A study of accuracy and repeatability. *Water Resour. Res.* 38(12):1309, doi:10.1029/2001WR000754.

Archie, G.E. 1942. The electrical resistivity log as an aid in determining some reservoir characteristics. *Trans. Am. Inst. Min. Metall. Pet. Eng.* 146:54–62.

Binley, A., P. Winship, L.J. West, M. Pokar, and R. Middleton. 2002. Seasonal variation of moisture content in unsaturated sandstone inferred from bore-

hole radar and resistivity profiles. *J. Hydrol.* 267:160–172.

Bosch, M. 2004. The optimization approach to lithological tomography: Combining seismic data and petrophysics for porosity prediction. *Geophysics* 69:1272–1282.

Cassiani, G., V. Bruno, A. Villa, N. Fusi, and A. Binley. 2006. A saline trace test monitored via time-lapse surface electrical resistivity tomography. *J. Appl. Geophys.* 59:244–259.

de Lima, O.A.L., and S. Niwas. 2000. Estimation of hydraulic parameters of shaly sandstone aquifers from geoelectrical measurements. *J. Hydrol.* 235:12–26.

Eppstein, M.J., and D.E. Dougherty. 1998. Efficient three-dimensional data inversion: Soil characterization and moisture monitoring from cross-well ground-penetrating radar at a Vermont test site. *Water Resour. Res.* 34:1889–1900.

Feng, S., and P.N. Sen. 1985. Geometrical model of conductive and dielectric properties of partially saturated rocks. *J. Appl. Phys.* 58:3236–3243.

Ferré, T.P.A., A.C. Hinnell, and J.B. Blainey. 2006. Inferring hydraulic properties using surface-based electrical resistivity during infiltration. *Leading Edge* 25:720–723.

French, H., and A. Binley. 2004. Snowmelt infiltration: Monitoring temporal and spatial variability using time-lapse electrical resistivity. *J. Hydrol.* 297:174–186.

Furman, A., T.P.A. Ferré, and G.L. Heath. 2007. Spatial focusing of electrical resistivity surveys considering geologic and hydrologic layering. *Geophysics* 72:F65–F73.

Green, W.H., and G.A. Ampt. 1911. Studies on soil physics: I. Flow of air and water through soils. *J. Agric. Sci.* 4:1–24.

Kowalsky, M.B., S. Finsterle, J. Peterson, S. Hubbard, Y. Rubin, E. Majer, A. Ward, and G. Gee. 2005. Estimation of field-scale soil hydraulic and dielectric parameters through joint inversion of GPR and hydrological data. *Water Resour. Res.* 41:W11425, doi:10.1029/2005WR004237.

Kunetz, G. 1966. Principles of direct current resistivity prospecting. *Geoexploration Monogr.*, Ser. 1, no. 1. Gebrüder Borntraeger, Berlin.

Lambot, S., M. Antoine, I. van den Bosch, E.C. Slob, and M. Vanclooster. 2004. Electromagnetic inversion of GPR signals and subsequent hydrodynamic inversion to estimate effective vadose zone hydraulic properties. *Vadose Zone J.* 3:1072–1081.

Oldenborger, G.A., M.D. Knoll, P.S. Routh, and D.J. LaBrecque. 2007. Time-lapse ERT monitoring of an injection/withdrawal experiment in a shallow unconfined aquifer. *Geophysics* 72:F177–F187.

Philip, J.R. 1969. Theory of infiltration. *Adv. Hydrosol.* 5:215–296.

Roy, A., and A. Apparao. 1971. Depth of investigation in direct current methods. *Geophysics* 36:943–959.

Rucker, D.F., and T.P.A. Ferré. 2004. Parameter estimation for soil hydraulic properties using zero-offset borehole radar: Analytical method. *Soil Sci. Soc. Am. J.* 68:1560–1567.

Schon, J.H. 1996. Physical properties of rocks: Fundamentals and principals of petrophysics. Elsevier, Amsterdam.

Shevnev, V., A. Mousatov, A. Ryjov, and O. Delgado-Rodriguez. 2007. Estimation of clay content in soil based on resistivity modelling and laboratory measurements. *Geophys. Prospect.* 55:265–275.

Singha, K., and S.M. Gorelick. 2005. Saline tracer visualized with electrical resistivity tomography: Field scale moment analysis. *Water Resour. Res.* 41:W05023, doi:10.1029/2004WR003460.

Singha, K., and S.M. Gorelick. 2006. Effects of spatially variable resolution on field-scale estimates of tracer concentration from electrical inversions using Archie's law. *Geophysics* 71:G83–G91.

Slater, L.D., and D.R. Glaser. 2003. Controls on induced polarization in sandy unconsolidated sediments and application to aquifer characterization. *Geophysics* 68:1542–1558.

Topp, G.C., J.L. Davis, and A.P. Annan. 1980. Electromagnetic determination of soil water content: Measurements in coaxial transmission lines. *Water Resour. Res.* 16:574–582.

Wait, J.R. 1982. *Geo-electromagnetism*. Academic Press, New York.

Warrick, A.W. 1993. Inverse estimations of soil hydraulic properties with scaling: One-dimensional infiltration. *Soil Sci. Soc. Am. J.* 57:631–636.

Warrick, A.W. 2003. *Soil water dynamics*. Oxford Univ. Press, New York.

Waxman, M.H., and L.J. Smits. 1968. Electrical conductivities in oil-bearing shaly sands. *Soc. Pet. Eng. J.* 8:107–122.